Models for analysing the economic impact of ore sorting, using ROC curves

by A. Drumond[1], A.L. Rodrigues[1], J.F.C.L. Costa[1], F.G. Niquini[1], and M.G. Lemos[2]

Affiliation:
[1]UFRGS/DEMIN, Porto Alegre RS, Brasil
[2]AngloGold Ashanti, Brazil

Correspondence to:
F.G.F. Niquini

Email:
fernanda.gontijo.fn@gmail.com

Dates:
Received: 6 Nov. 2023
Revised: 28 Feb. 2024
Accepted: 5 Apr. 2024
Published: July 2024

How to cite:
Drumond, A., Rodrigues, A.L., Costa, J.F.C.L., Niquini, F.G., and Lemos, M.G. 2024. Models for analysing the economic impact of ore sorting, using ROC curves. *Journal of the Southern African Institute of Mining and Metallurgy*, vol. 124, no. 7. pp. 397–406

DOI ID:
http://dx.doi.org/10.17159/2411-9717/3186/2024

ORCID:
A. Drumond
http://orcid.org/0000-0002-5383-8566
A.L. Rodrigues
http://orcid.org/0000-0003-4524-4087
J.F.C.L. Costa
http://orcid.org/0000-0003-4375-370X
F.G. Niquini
http://orcid.org/0000-0003-1872-1466
M.G. Lemos
http://orcid.org/0000-0002-9629-3332

Abstract

The past decade has seen a renewed possibility of using machine learning algorithms to solve a large collection of problems in several fields. Data acquisition for mining operations has increased with the growth in sensor-based technologies, and therefore the amount of information available for mining applications has dramatically increased. Ore sorting equipment is available for separating ore from waste based on differences in physical properties detected by a real-time analyser. The separation efficiency depends on the contrast in these properties. In this study we investigate the application of machine learning models trained using data from the output of a dual-energy X-ray ore sorting apparatus at a gold mine. The particles were first hand-sorted into ore and gangue classes based on their mineralogical composition. Classification models were then used to help decide the balance between the number of true and false positives for ore in the concentrate, with a view to economic parameters, using their receiver operator characteristic (ROC) curves. The results showed AUC (area under the ROC curve) scores of up to 0.85 for the classification models and a maximum reward condition F_{pr}/T_{pr} around 0.5/0.9 for a simplified economic model.

Keywords

sensor-based sorting, machine learning, receiver operating characteristic

Introduction

Mineral deposits are natural anomalies described by their specific physical and chemical properties. These properties directly affect the performance of mining and ore processing equipment. It is desirable to understand the relationships between the mineralization characteristics and the process used in ore dressing. Geometallurgy provides the means to identify these relationships and mathematically model the influence of these variables on the metallurgical response. According to Lechuti-Tlhalerwa, Coward, and Field (2019), 'Geometallurgy is an interdisciplinary field aimed at describing potential ore deposits in terms that mine planners and economists can use to design and run profitable mining operations'.

Ore sorting by mechanical means is used for the preconcentration of mineral particles. Sorting could be used for various purposes, ranging from initial waste removal to downstream processing. As a unitary processing operation, ore sorters require materials with certain characteristics. Most ore sorting applications require coarse mineral grains and a low flow rate to operate properly. According to Wills and Finch (2015), ore liberation is an important restriction for this technology. The typical throughput per machine ranges from 25 t/h at 25–5 mm particle size to 300 t/h for 300–80 mm. Despite some technological pitfalls, there are numerous advantages of this technology, including significant energy and water savings (Manouchehri, 2003).

Ore sorting equipment can have different or multiple sensors for detecting physical properties (Manouchehri, 2003). A schematic of an X-ray sorting machine is shown in Figure 1. The material is initially fed according to granulometric constraints in step 1. For practical purposes, fines are commonly removed to avoid their interfering with the physical measurements made by the X-ray sensors. The ore is transported by means of a vibratory belt, forming a single layer of particles to allow readings to be acquired from every individual particle. In step 2, particles pass by X-ray sensors and are analysed based on the intensity of their X-ray transmissibility. The physical measurements of each particle are computed and analysed. According to a pre-adjusted mathematical model, the particles are accepted or rejected from the stream in the separation chamber, by a pneumatic apparatus flaps.

There are few published studies in the field of ore sorting specifically focused on ore classification. Von Ketelhodt (2009) tested the viability of optical sorting to process low-grade gold ore that had been

stockpiled for a long time. Von Ketelhodt and Bergmann (2010) employed dual-energy X-ray sensors to concentrate coal, thus reducing downstream water consumption. Dual-energy X-ray ore sorting has also been applied for the classification of rare earth elements (REEs) (Veras et al., 2020). In addition to X-ray techniques, sensors based on the near-visible spectrum have been utilized. Tusa et al. (2020) presented hyperspectral results using visible to near-infrared (VNIR) and short-wave infrared (SWIR) sensors, while Gülcan (2020) evaluated borate sorting using near-infrared sensors.

Lessard, de Bakker, and McHugh. (2014) conducted an extensive study on the economic impact of using dual-energy X-ray transmission (DE-XRT_ ore sorting of molybdenum ore. They explored which parameters yielded the highest sensitivity for the equipment in order to achieve the best economic outcome.

Li et al. (2020) investigated the use of X-ray fluorescence (XRF) sorting on samples from a porphyry copper mine. XRF is a surface analysis technique, and this work was conducted in a well-controlled laboratory environment. The study correlated economic return (net smelter return, NSR) with the cut-off grade.

In this study we investigate the possibilities of modelling the data output from a DE-XRT ore sorting machine (a TOMRA PRO Secondary) for the case of a gold deposit. The output data is multivariate, which is appropriate for machine learning techniques. After training a machine learning model, another parameter (the threshold) is taken into account, which is linked to the true positive rate (the proportion of ore correctly identified by the model relative to the total ore in the data-set) and false positive rate (the proportion of gangue misidentified as ore relative to the amount of gangue in the data-set).

This parameter allows the decision-maker to choose to include more ore in the concentrate, but at the expense of also including more gangue (resulting in dilution). Optimizing this parameter is crucial for achieving the best economic benefits from the process, which aligns with one of the objectives of this paper and is related to a question raised in the literature by Lessard, de Bakker, and McHugh (2014).

Dual-energy X-ray transmission

A thorough understanding of the sensor variables and operation is necessary beforehand. In the context of this study, the present findings are related to dual-energy X-ray absorptiometry applied to ore from gold deposits. According to Strydom (2010), particle classification using X-ray transmission sensors is based on the differences in the X-ray absorption of the grains. The absorption of X-rays in turn depends on the atomic numbers of the elements forming the minerals. Each particle is penetrated by X-rays and the difference between the transmitted and absorbed energy results in a contrast of brightness from the various particles. Furthermore, the attenuation of the X-ray emission depends on the grain thickness as well. The phenomenon referred to as transmission damping can be explained by X-ray transmission theory. Lambert's law indicates that transmission damping is a function of the density and thickness of the material:

$$I_{det} = I_0 e^{-\mu(\delta)\rho d} \quad [1]$$

where I_{det} is the detected intensity, I_0 is the intensity of the undisturbed beam, $\mu(\delta)$ is the mass absorption coefficient, ρ is the density of the solid, and d is the thickness of the irradiated material.

Lambert's law can be applied to dual-energy absorption by transmitting high- and low-energy X-ray beams. An advantage is that the particle thickness can be determined using Lambert's law for the high- and low-energy levels. Jong and Harbeck (2005) showed that the relationship between the detected intensities results in a constant, C_m, which depends only on the properties of the material and the chosen wavelength (Equation [2]). Common values of C_m are related to the atomic number for a specific element.:

$$\frac{I_1}{I_2} = e^{-\Delta\mu\rho d} = (e^{-\Delta\mu\rho})^d = C_m^d \quad [2]$$

Harbeck (2004) demonstrated that different minerals can be distinguished by comparing the degree of transmission of X-rays through the particles at two different energy levels. By examining the brightness levels produced by materials for two different X-ray channels, it is possible to visually interpret a density model.

Figures 2a and 2b show the X-ray images for different channel frequencies. Different wavelengths have different transmission values through the mineral particle: high frequencies penetrate the particle less than low frequencies. Figure 2c shows a scatter plot for the two channel readings (high and low frequency) at every pixel within the X-ray image according to the intensity values of channels with high and low frequencies. Pixels below the calibration curve are considered as low-density pixels, and those above the curve as high-density. The pixels can be counted as the indicator values of high and low densities.

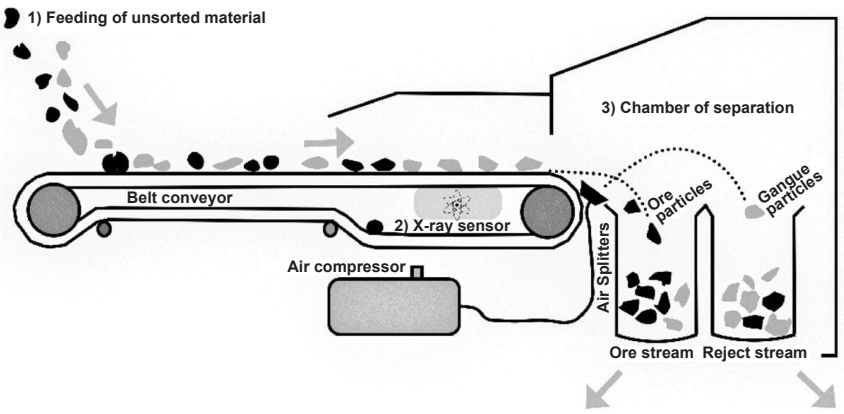

Figure 1—Schematic of an X-ray sorter. (1) The particles are fed into the equipment so as to form a single layer with no overlap between particles. (2) The electromagnetic sensor, where the X-ray waves are generated and transmitted through the particles. The equipment records and analyzes the X-ray images. (3) The separation chamber, where airgun blasts segregate the particles based on their classification as ore or gangue

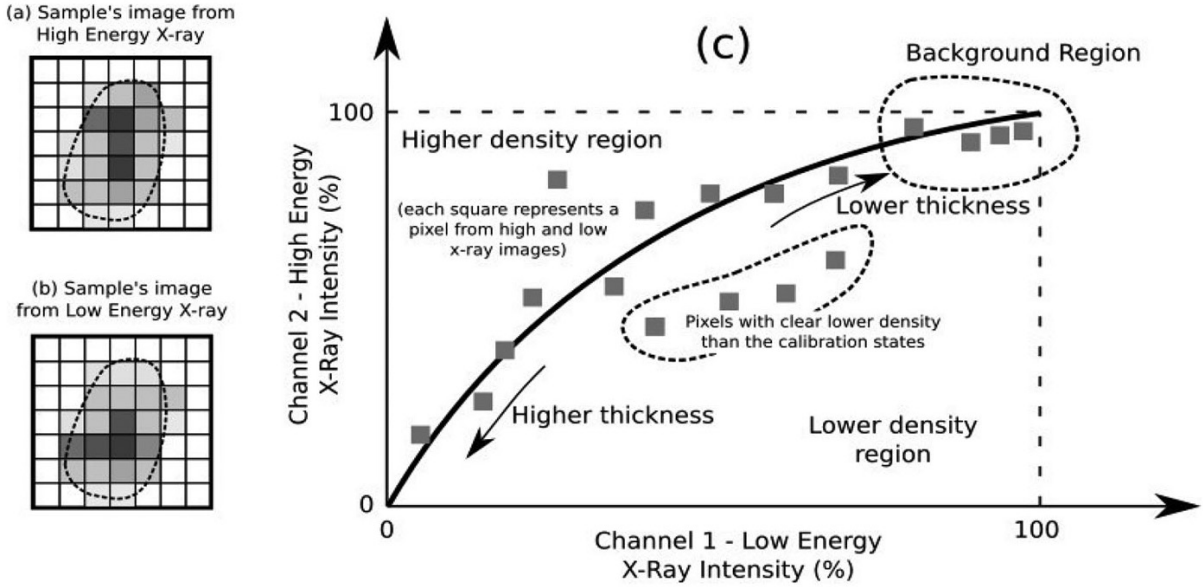

Figure 2—(a) High- and (b) low-energy X-ray images. Each pixel represents the X-ray transmission intensity in greyscale for the two energy levels (frequencies) in the area. (c) Each pixel is represented using the transmission in high energy as the y-value and the transmission in low energy as the corresponding x-value. The grey squares represent the readings from each pixel in (a) and (b) for the two channels. These points are scattered around the previously calibrated curve (continuous black line) for a given mineral. The decision on whether a particle is mineral or gangue is made by comparing the pixel readings from (c) to the calibrated curve

A filtering process might be needed for the data collected by the sensors, as a thick gangue particle can provide similar readings as a thick ore grain.

The data output from the sorter maps four regions: high, medium, low, and dark. To calculate density models for mineral particles, the calibration curve must be adjusted to fit a threshold limit based on several particle measurements. For example, a density curve of 60% means that 60% of the total samples from a given mineral are plotted below the curve.

The use of machine learning

According to Webb and Copsey (2011), machine learning and pattern recognition developed as an interdisciplinary subject, covering statistics, engineering, computer science, psychology, and physiology, among others. One special characteristic of machine learning modelling is dealing with multivariate problems. The present study requires that a decision must be made about each analysed particle using a multidimensional input vector of data readings representing the corresponding sample. Supervised machine learning methods are appropriate for addressing these multidimensional decision problems when prior sampled data, designated by experts as ore and gangue through hand sorting, is available.

A supervised model trained with ore/gangue designated data can be used to make decisions about whether a new, unknown sample is ore or not, and to present the degree of certainty for this prediction. Supervised algorithms could be used in two main applications: for regression and for classification. The first relates to real target values, whereas the second relates to a categorical value. For a binary output, like ore/gangue, this output is represented by (1) when a particle is ore and (0) when the particle is gangue. Ore sorting can be viewed as a traditional classification problem, since ore and gangue particles are classified into concentrate or the waste streams (Figure 3).

All classification outcomes can be summarized in the confusion matrix (Table I), which provides a comprehensive overview of true positive, true negative, false positive, and false negative classifications.

Machine learning metrics can be applied to assess the performance of an ore sorting model. These metrics are derived from the confusion matrix, which summarizes the classification results. Equations [3] to [6] present some of the key metrics used in this assessment:

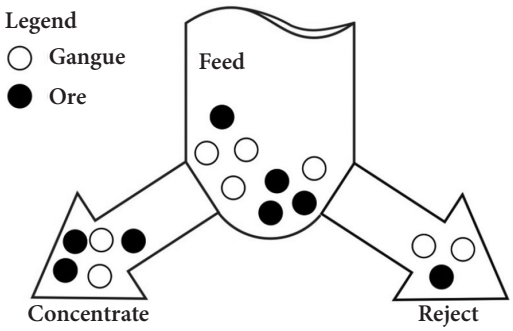

Figure 3—Separation of the feed into concentrate and waste (tailings) streams. Since the concentration process is not perfect, some waste particles could be directed to the concentrate

Table I

Confusion matrix for ore sorting products. Mineral particle in rows and downstream definition in columns. The true positive values and true negative values are considered to be the particles that are correctly directed to their desired downstream destinations. False positives and false negatives indicate incorrectly classified particles

Type	Concentrate	Waste
Ore	True positive	False negative
Gangue	False positive	True negative

$$T_{pr}, \text{ Recall or Sensitivity} = \frac{T_p}{T_p+F_n} = \frac{Ore\ particles\ predicted\ as\ ore}{All\ ore\ particles} \quad [3]$$

$$F_{pr} = 1 - \text{Specificity} = \frac{F_p}{F_p+T_n} = \frac{Waste\ particles\ predicted\ as\ ore}{Total\ waste\ particles} \quad [4]$$

$$\text{Accuracy} = \frac{T_p+T_n}{T_p+T_n+F_p+F_n} = \frac{Particles\ correctly\ classified}{Total\ number\ of\ particles} \quad [5]$$

$$\text{Precision} = \frac{T_p}{T_p+F_p} = \frac{Ore\ particles\ classified\ as\ ore}{All\ particles\ classified\ as\ ore} \quad [6]$$

where T_p is true positive, F_p is false positive, T_n is true negative, and Fn is false negative.

In the context of ore sorting classification, terminology that aligns with machine learning concepts is not well-established in the literature. To address this gap and facilitate understanding, we propose the following definitions:

- *Concentrate ore grade*: The proportion of ore in the concentrate stream. This concept is analogous to precision metrics used in machine learning classification problems.
- *Recovery*: The metric which measures the proportion of ore particles in the training set that is sent to the concentrate. This definition is also called the true positive rate (T_{pr}) in machine learning classification metrics.

Proposing a mathematical model for particle recovery and the ore grade in the concentrate allows the modeller to manage specific conditions related to the equipment to achieve the desired characteristics for the process.

In assessing the performance of mathematical models for ore sorting, the receiver operator characteristic (ROC) curve serves as a crucial tool. This curve provides insights into the relationship between false positive rate (F_{pr}) and true positive rate (T_{pr}), aiding in the evaluation of model effectiveness. The ROC curve (Figure 4) establishes, for a given trained model, a relationship between the false positive rate (F_{pr}, on the x-axis) and true positive rate (T_{pr}, on the y-axis). The area under the ROC curve (AUC score) provides a comprehensive measure of the model's performance, ranging from 0 to 1. A higher AUC score indicates better predictive accuracy.

The threshold is the parameter which controls the trade-off between the T_{pr} and the F_{pr} given a trained model. For example, for an input particle, the model predicts a 75% probability of it being ore. If the threshold chosen is 50%, the prediction will be ore. If the threshold selected is 90%, the prediction would be gangue. Changing the threshold results in a repositioning along the model, moving within the ROC curve and effectively implementing a trade-off between the amount of gangue in the concentrate and the quantity of ore sent to the reject stream. If the operator wants to value the true positive rate (when the model answers ore, it should really be ore!) the threshold must be set to a higher value, 98% for instance. In this case, the model will behave as point 1 in Figure 4c. The opposite case is when the threshold is set to 0%, returning all the predictions as ore regardless of the particle input. This case is represented by point 4 in Figure 4c. Figures 4a and 4b show the definitions of the true positive rate (T_{pr}, associated with the ore recovery) and false positive rate (Fpr).

Variables, preprocessing phase, and ore definition

Variables and preprocessing phase

The variables employed in the modelling will be called 'features'. In this study a mineral sample has 17 features (Figure 5): 16 continuous numerical features related to three different density model calibration curves and a categorical feature corresponding to the origin of the sample in the orebody. The preprocessing phase comprises two stages. The first stage involves replacing the

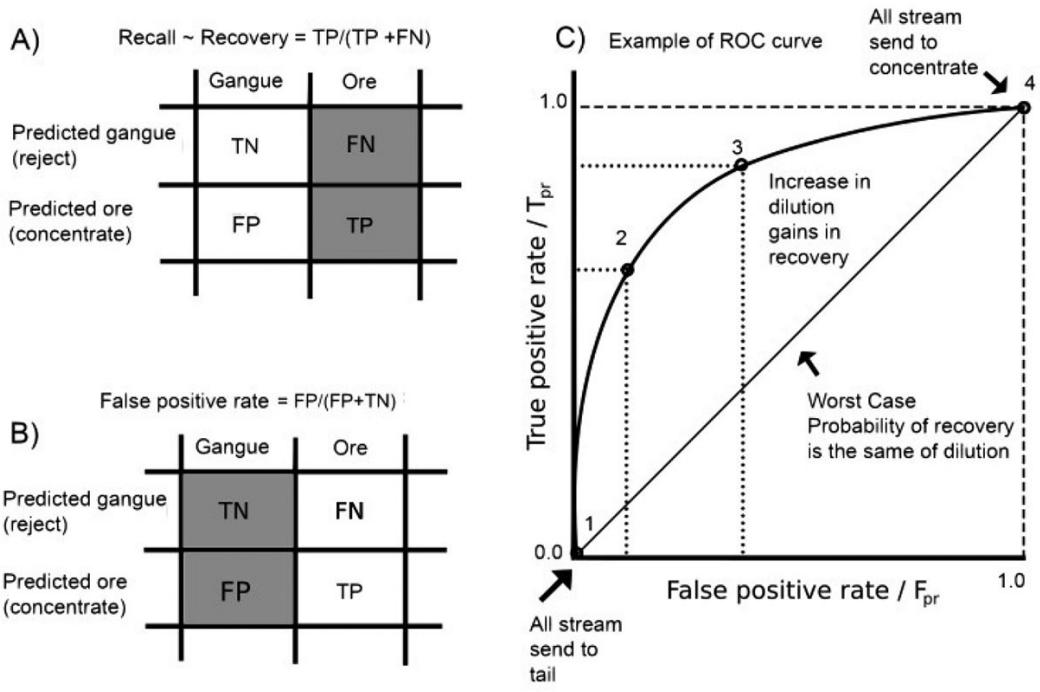

Figure 4—Example of a ROC curve. The x-axis and y-axis are physically related to properties in the ore sorting equipment. (A) shows the recall and its physical interpretation: the ore portion in concentrate. (B) shows the false positive rate and its physical interpretation: the amount of waste in the concentrate relative to the total amount of waste in the feed. (C) Two different ROC curves: the straight line is the worst model where all predictions are realized randomly. Points 1 and 4 represent the total stream deviations respectively to the tailings and to the concentrate

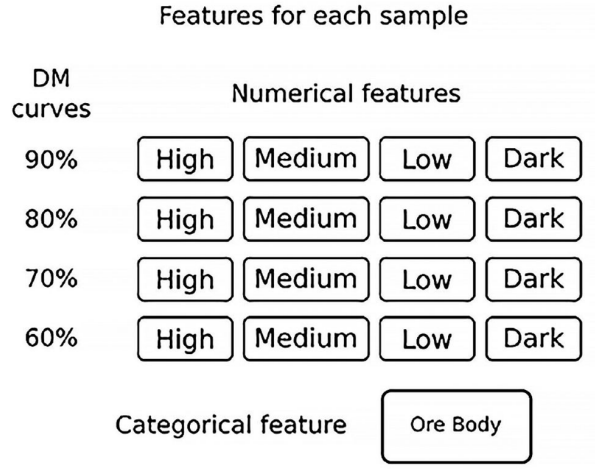

Figure 5—The features used in the study comprise four numerical features contributed by each DM calibration curve, resulting in a total of 16 continuous numerical features. Additionally, the categorical feature representing the origin of the sample in the orebody is replaced by the probability of each class. As a result, each mineral sample is represented by a vector with 17 entries

numerical features corresponding to the absolute number of pixels in each 'band' with the pixel proportion in each band for each sample. For example, a sample in DM-70 with 40 pixels in high, 20 in dark, 10 in medium, and 30 in low, will be transformed into proportions (0.4, 0.2, 0.1, 0.3) respectively, given that the total number of pixels for this sample is 100.

In the second stage of preprocessing, standardization is applied to each feature and the categorical variable is replaced by the probability of each class in the data-set. Figure 5 lists the numerical features and the categorical feature used to perform the training.

Ore definition

To be classified as ore, a particle must exhibit either the target mineralogy (such as sulphides, quartz, or fine arsenopyrite) or a grade above the cut-off value of 0.4 ppm. Figure 6 depicts the ore class, illustrating the criteria used for classification. This indicator variable, based on the specified criteria, serves as the response variable for the supervised learning classification algorithms.

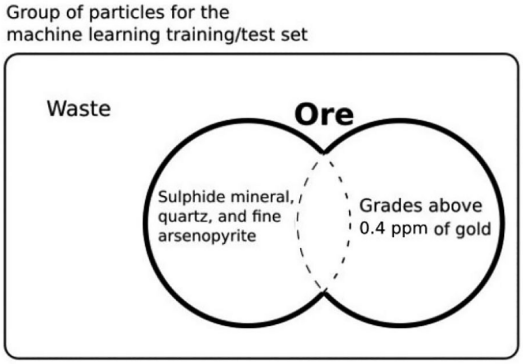

Figure 6—The definition of the ore class, which is determined based on mineralogy or gold grade. This class serves as the response variable in the ore sorting classification process. Particles are classified as ore if they exhibit the target mineralogy or have gold grades above the specified cut-off value. Any particles not meeting these criteria are classified as waste

Hand sorting and database creation

The process for calculating the indicators of high, medium, low, and dark proportions according to each density model is shown in Figure 7. The process starts by sampling different regions from the mineral deposit, so that each particle can later be individually analysed according to the X-ray measurements. The images composed of the channels of high and low energy transmitted along the particles are simulated to obtain the proportion of indicators (high, medium, and low densities) for each density model considered. The final supervised database is composed of measurements of the properties of individual rock particles, including the calculated indicators of high, medium, low, and dark proportions according to each density model.

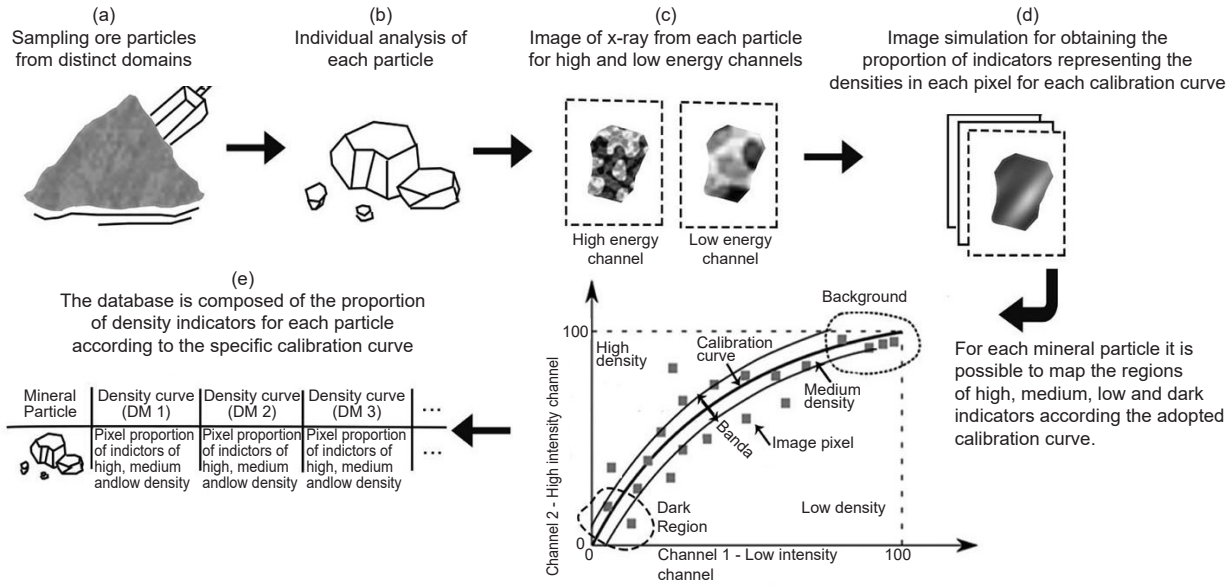

Figure 7—The process of creating the database for ore particles. (a) Particles are sampled from various regions in the mineral deposit. (b) Each particle is individually coded and analysed. (c) Two images are generated based on the high and low channel frequencies from the X-rays. (d) These images are simulated using different density models. The proportions of high, medium, low, and dark pixels are then computed. (e) The final database is composed of the proportion of density indicators for each particle, according to the specific calibration curve

In this study, the labels high, low, medium, and dark correspond to density regions, while DM% represents the density model used. Additionally, a categorical variable representing the mined orebody associated with each particle was introduced. This categorical variable has six possible outcomes. To incorporate the categorical variable into the modelling process, it was encoded into a frequency-based representation. This encoding method assigns numerical values to each category based on their frequency of occurrence in the data-set.

The data acquisition, calibration, and sampling processes were carried out by the technical staff of a mining company in Brazil, as documented in studies by Magalhães et al. (2019) and Dumont, Lemos Gazire, and Robbens (2017). This study focuses on analysing the output data from the ore sorting equipment using samples from these deposits.

Proposing a decision criterion

After training a machine learning model and obtaining the ROC curve, determination of the optimal combination of true positive rate (T_{pr}) and false positive rate (F_{pr}) for the most economical decision depends on various factors, including the value of the concentrate and associated costs. In this section we introduce an economics-based decision model.

To illustrate this decision-making scenario, we present a simple reward (benefit) function model. Unlike a loss function, which aims to be minimized, a reward function seeks to be maximized to increase profit.

Consider an amount M of material to be analysed and processed by the ore sorting equipment. The ore sorting model is already trained and the parameters chosen. The necessary parameters are presented as the general true positive rate T_{pr} and false positive rate F_{pr}.

Although the sorter operates on a particle basis (not exactly mass), one can create a mathematical formulation considering mass when using the hypothesis that all particles have the same mass, which may be some statistical mean mass established from field data. This will be the case for the formulation in this section.

This mass M to be processed is divided into ore (M_o) and gangue (M_g) masses, so that $M = M_o + M_g$. The amount of material which is selected as ore by the model in the equipment is given by $M_oT_{pr} + M_gF_{pr}$ and the amount discarded by $M_gT_{nr} + M_oF_{nr}$. The true negative rate T_{nr} and the false negative rate Fnr are given by:

$$T_{nr} = Specificity = 1 - F_{pr} \quad [7]$$

$$F_{nr} = 1 - T_{pr} \quad [8]$$

The balance is the reward from the correctly accepted gold (M_oT_{pr}), the cost of processing all accepted (as ore) material $M_oT_{pr} + M_gF_{pr}$, and the total cost of processing the rejected material $M_gT_{nr} + M_oF_{nr}$. This simplified model is based on the benefit of the correctly predicted ore and the relative difference in costs between processing some amount of material as ore or as waste. Expressing this reward function in an equation leads to:

$$\begin{aligned} R(T_{pr},F_{pr}) &= BM_oT_{pr} - C_pM_oT_{pr} - C_pM_gF_{pr} - C_{p2}M_gT_{nr} - C_{p2}M_oF_{nr} \\ R(T_{pr},F_{pr}) &= BM_oT_{pr} - C_pM_oT_{pr} - C_pM_gF_{pr} - C_{p2}(1-F_{pr})M_g - C_{p2}(1-T_{pr})M_o \\ R(T_{pr},F_{pr}) &= (B - C_p + C_{p2})M_oT_{pr} + (C_{p2} - C_p)M_gF_{pr} - C_{p2}(M_g + M_o) \end{aligned} \quad [9]$$

where B is a parameter related to the financial gain from the specific mineral (gold in this case), C_p is a parameter connected to the processing costs of the accepted material, and C_{p2} is another parameter linked to the processing costs of the rejected material. All these three parameters are in units of dollars per unit mass, e.g. US$ per ton.

Rewriting the reward expression (Equation [9]) yields:

$$\begin{aligned} \frac{R(T_{pr},F_{pr})}{M} &= (B - C_p + C_{p2})\frac{M_oT_{pr}}{M} + (C_{p2} - C_p)\frac{M_gF_{pr}}{M} - \frac{C_{p2}(M_g + M_o)}{M} \\ r(T_{pr},F_{pr}) &= (B - C_p + C_{p2})m_oT_{pr} + (C_{p2} - C_p)m_gF_{pr} - C_{p2} \end{aligned} \quad [10]$$

where m_o is the fraction of ore in the total mass, M_o/M, and m_g is the fraction of gangue in the total mass, M_g/M. The reward function $r(T_{pr},F_{pr})$ is expressed in the same units as the parameters B, C_p, and C_{p2} (for example US$/t) and indicates the amount of money (US$) for an amount of material fed to the ore sorter (t).

Note that $r(T_{pr}, F_{pr})$ depends on two variables. A trained model will yield the relationship between these two variables, which is given by the ROC curves shown previously. When establishing a reward function for an ROC curve, the reward function will take the form $r(F_{pr})$.

Although the presented reward function model is simple and limited, it serves as a starting point for decision-making in ore sorting processes. In real mining operations, it is possible to develop a more comprehensive and specific reward function tailored to the unique characteristics of the operation.

One notable factor not accounted for in the cost model is the operational cost of the ore sorting equipment, which includes energy consumption and maintenance costs (Lessard, de Bakker, and McHugh, 2014). However, this cost was intentionally omitted from the model, as its value does not significantly depend on the choice of T_{pr} and F_{pr}.

In the next step of the analysis, two additional quantities will be calculated and incorporated into the decision-making model. The first is the total mass of concentrate output from the ore sorting process given a specific F_{pr}. The second is the grade of the concentrate obtained at that F_{pr}. These additional metrics will provide valuable insights into the operational boundaries and help optimize planning for the ore sorting operation.

The total mass in concentrate is:

$$\begin{aligned} Total\ mass \in concentrate &= M_oT_{pr} + M_gF_{pr} \\ \frac{Total\ mass \in concentrate}{M} &= m_oT_{pr} + m_gF_{pr} \end{aligned} \quad [11]$$

where the total mass in the concentrate is given in relation to the mass fed to the ore sorting (M).

The ore grade in the concentrate is given by:

$$\begin{aligned} Ore\ grade \in concentrate &= \frac{M_oT_{pr}}{M_oT_{pr} + M_gF_{pr}} \\ Ore\ grade \in concentrate &= \frac{1}{1 + \frac{m_g}{m_o}\frac{F_{pr}}{T_{pr}}} \end{aligned} \quad [12]$$

The question may arise as to when it would be valuable to create a figure illustrating ore mass recovery as a function of F_{pr}. Interestingly, such a figure has already been produced in the form of the ROC curve (Figure 14). In the ROC curve, the y-axis represents T_{pr}, which is equivalent to Recall in machine learning terminology. This Tpr value can be interpreted as the total amount of ore in the deposit that can be recovered at a given F_{pr}.

The purposes illustrated in this section were produced and commented mimicking a long-term mine planning analysis. But it would be trivial to change the timeframe planning. By changing m_o

and m_g according to the deposit estimates in a given time period, the models do not need to be retrained if the original training set is already statistically representative of the deposit as a whole. Even the other parameters, such as C_p and C_{p2}, can be re-estimated for another time period. For further development of economic models using ROC curves one can refer to Ooms et al. (2010). The results of the economic criteria are presented in a later section.

Results and discussion

Training the ML algorithms, model selection phase

Seven machine learning classification algorithms were tested to build the classification model: random forest (Breiman, 2001), logistic regression (Cox, 1958), K-nearest neighbours (KNN with K = 6) (Cover and Hart, 1967), support vector machine (SVM) with radial basis function (RBF) kernel and linear kernel (Boser, Guyon, and Vapnik, 1995), Gaussian naive Bayes (Duda and Hart, 2001), and AdaBoost (Freund and Schapire, 1996).

The data-set was divided into two parts: 1160 records (approximately 70%) were used in the model selection phase, and the remaining 498 records were held back for evaluating the best-selected model. During the model selection phase, a stratified K-fold cross-validation approach with K = 5 was employed. The evaluation metric used was the AUC score (area under the ROC curve). The results are presented in Figure 8.

Among the tested algorithms, random forest achieved the highest AUC score of 0.798, followed closely by SVM with RBF kernel (0.794) and KNN with K = 6 (0.791). On the other hand, logistic regression, Gaussian naive Bayes, and SVM with linear kernel exhibited poorer performances. All models were initialized with standard parameters from the *Scikit-Learn* implementations.

Figure 9 displays the ROC curves for all selected machine-learning models. To provide context, a straight line representing random predictions is plotted as a reference. The ROC curve is a valuable measure that assesses the overall quality of a given model across all possible values of F_{pr} and T_{pr}. For each trained model, varying the threshold (as discussed previously) results in different F_{pr}/T_{pr} values. By visually comparing the ROC curves, different models can be assessed and compared. The AUC scores, presented in Figures 9 and 10, represent the area under each ROC curve. The AUC score condenses the model's performance into a single value, facilitating comparative analysis. Comparison of the AUC scores and visual inspection of the ROC curves shows that the random forest is the model with the best performance.

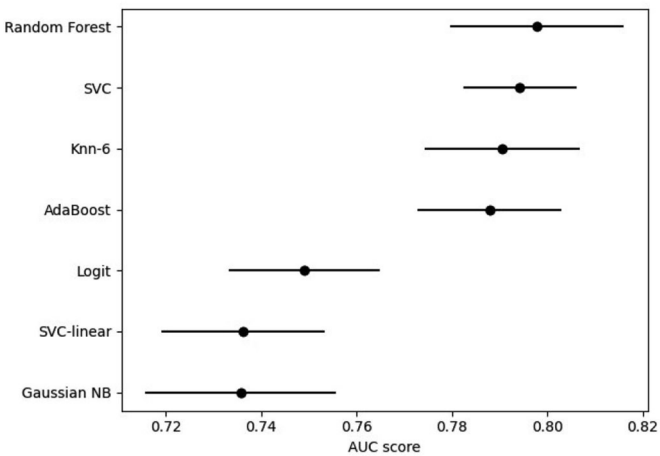

Figure 8—Model selection using AUC mean scores for 5-fold cross-validation with confidence interval of 69% (one standard deviation)

Assessment of performance with evaluation data

After selecting the model, it is crucial to verify its performance using the evaluation data-set to ensure its ability to generalize to new, unseen records. The results presented in Figure 10 indicate an AUC score of 0.783 for the selected random forest model.

It is important to note that using the evaluation set to select the best-performing model among previous candidates can lead to overfitting. Overfitting occurs when the model performs exceptionally well on the evaluation set but fails to generalize to new data. This phenomenon, also known as second-order overfitting (Reunanen, 2012), emphasizes the importance of robust evaluation procedures to avoid misleading conclusions.

Results of the economic model

In the economics-based model, the parameters outlined in Table II were utilized. To cover a range of classification methods, several techniques were explored, including random forest, decision trees (Quinlan, 1986), linear discriminant analysis (Fisher, 1936), Gaussian naive Bayes, K-nearest neighbours, logistic regression, neural networks (McCulloch and Pitts, 1943; Bishop, 2006), and support vector classifier.

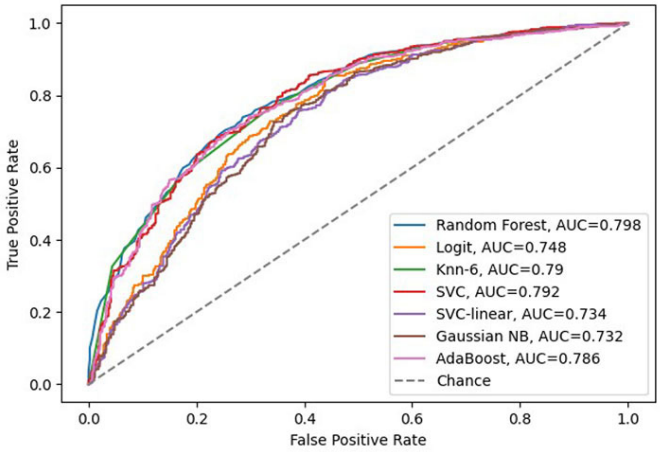

Figure 9—Receiver operating characteristic (ROC) curves for all supervised machine-learning algorithms utilized in the model selection phase. Among the algorithms tested, random forest achieved the highest area under the curve (AUC) score, with a value of 0.793

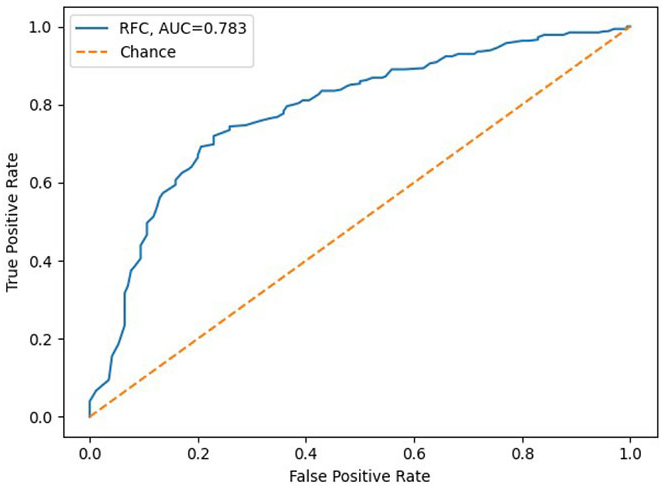

Figure 10—Result for the random forest model using the previously unseen evaluation data-set

Table II

Parameters used for the economic model

Parameter	Value	Observations
m_o	1.0×10^{-6}	1 ppm
m_g	9.99999×10^{-1}	$m_g = 1 - m_o$
B	60 000 US$/kg	market price
C_p	10 US$/t	
C_{p2}	1 US$/t	

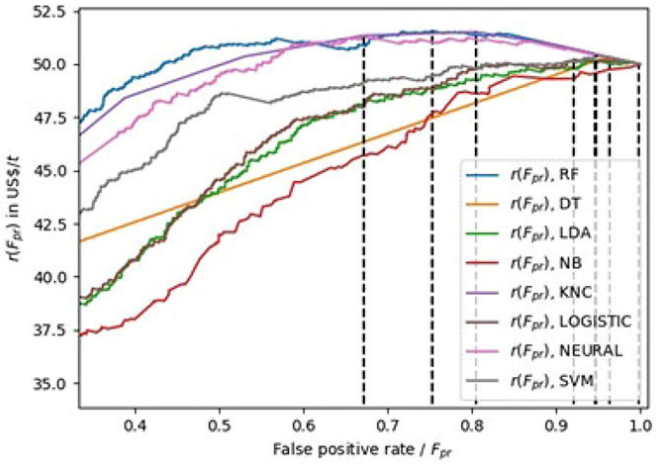

Figure 11—Comparison of the rewards $r(F_{pr})$ for all trained models. The maxima of each curve are marked with a vertical dashed line. The highest reward is from the RF model at F_{pr} = 0.75 and r(0.75) = 51.6 US$/t

Figure 11 compares the reward functions for all trained models using $B = 6 \times 10^6$ referenced in Table II. The best reward is from the RF model, when $F_{pr} = 0.75$ and $r(0.75) = 51.6$ US$/t. It shows good general performance in discriminating ore and waste, which can be seen as the $r(F_{pr})$ curve for RF is overall above the others (the AUC scores in Figure 14 also show the same pattern). This offers the decision-maker other strategies for using the reward $r(F_{pr})$. For example, the point in the RF reward curve at $F_{pr} = 0.47$ and $r(0.47) = 50.8$ yields almost the same reward as the maximum (51.6), but with a significantly lower value of $F_{pr} = 0.47$, which can lead to a compelling cut in costs not taken into account in the economic model. So, the reward curves must be seen as a tool to help in a decision, and not an automatic method to extract the maxima.

Another outcome from Figure 11 is the importance of a well-trained model. A poorly calibrated model embedded in the ore sorting decision can lead to a significantly lower profit, from 30% to 10% less, depending on F_{pr}.

Figure 12 shows the total mass in the concentrate relative to the mass M fed into the ore sorter. The curves for all models are collapsed to a visually straight line due to the low proportion of ore in the mass fed (1 ppm). In this case, Equation [13] is dominated by the term $M_g F_{pr}$, which is a first degree monomial considering the variable F_{pr}. For an increasing value of mo the curves will take another geometrical form.

The relationship shown in Figure 12 is a convenient method to establish boundaries on F_{pr} for the desired effect. For example, if the operator wants to reduce the mass in the concentrate (by being more selective), then the initial value for F_{pr} can be estimated using this graph.

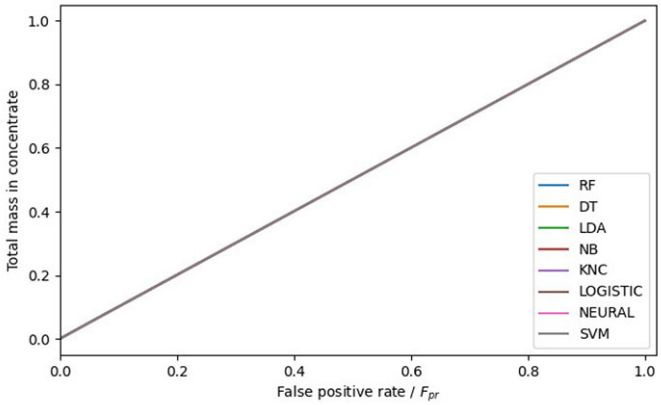

Figure 12—Total mass present in concentrate relative to the mass M fed to the sorter. The curves appear to be linear due to the small value of m_o, given the definition of the mass in concentrate $m_o T_{pr} + m_g F_{pr}$

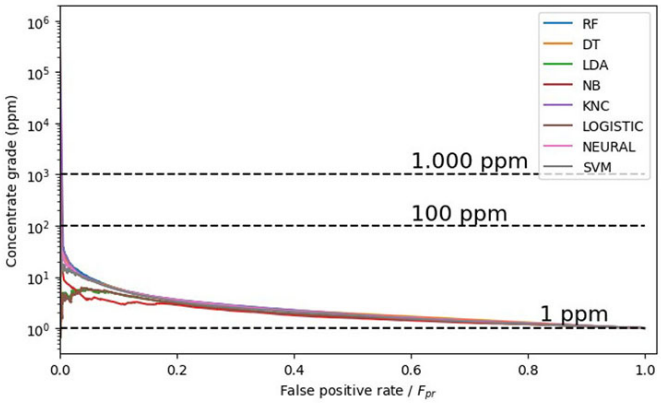

Figure 13—Concentrate grade vs F_{pr}. When $F_{pr} \to 0$, the grade tends to 1, i.e., the concentrate is almost exclusively ore. When $F_{pr} \to 1$ the concentrate grade approaches m_o. Horizontal dashed lines mark grades at 1000 ppm, 100 ppm, and 1 ppm

Figure 13 shows the variation in concentrate grade for different values of F_{pr}. At the lowest values of F_{pr} the concentrate grade is approximately 1. However, in this case the concentrate mass is near zero (Figure 12). When F_{pr} approaches 1 the concentrate grade tends to the ore grade of M, which is m_o (1 ppm). As stated before, when $F_{pr} = 1$ all the material goes to the concentrate.

To illustrate the application of the findings from Figures 9, 12, and 13, consider a scenario where the false positive rate (F_{pr}) is set to 0.5 and the random forest (RF) model is employed. According to the ROC curve (Figure 9), with an Fpr of 0.5, approximately 94% of the ore will be recovered from the total mass (M) fed into the ore sorting process. Referring to the total mass curve in Figure 12, the total mass of concentrate obtained will be approximately half of the mass (M) fed into the sorting process. Finally, using the concentrate grade curve in Figure 13, at an Fpr of 0.5, the average grade of the concentrate will be approximately 1.8 ppm. This demonstrates how the information from Figures 9, 12, and 13 can be integrated to inform decision-making, allowing operators to assess and optimize ore recovery, concentrate mass, and concentrate grade based on their specific objectives and constraints.

Conclusions

The introduction of innovative ore-sorting equipment presents a promising opportunity for the mining industry, offering the potential to enhance mineral recovery while reducing operational

costs. Central to this improvement is the adaptive adjustment of the sensor decision model within the equipment. In this paper we have shown how multivariate models, particularly in the context of machine learning, can leverage the rich output variables from ore sorting to optimize model parameters, taking economic considerations into account.

By employing a simple profit-cost model, derived from the receiver operator characteristic (ROC) curve of a machine learning model, economic aspects are quantified to inform decision-making. Additionally, methodologies for modelling ore recovery, concentrate mass, and ore grade in the concentrate are provided. These resources serve as valuable tools to guide decision-makers, facilitating informed choices rather than automated decisions.

The multivariate modelling phase utilizes data output from the ore sorting equipment, albeit without capturing the full richness of dual-energy X-ray data for each pixel. This presents an opportunity for further enhancement, as leveraging raw dual-energy X-ray data could potentially improve modelling accuracy. Such improvements can be seamlessly integrated into the existing work flow outlined in this paper, allowing for economic-based decisions based on updated ROC curves.

To maximize the potential of this approach, it is recommended that ore sorting equipment manufacturers consider implementing interfaces capable of accepting models trained in high-level programming languages such as Python. This would enable seamless integration of advanced modelling techniques into the ore sorting process, further enhancing its efficiency and effectiveness.

Acknowledgements

This research was supported by Coordenação de Aperfeiçoamento de Pessoal de Nível Superior – Capes, AngloGold Ashanti Brazil and Fundação Luiz Englert.

Conflict of interest

The authors declare that they have no conflict of interest.

Author statement

D.A.D.: Conceptualization, methodology, software, investigation, writing; A.L.R.: Methodology, software, investigation, writing, validation, visualization
J.F.C.L.C.: Validation, resources, supervision, funding acquisition;
F.G.F.N.: Writing, validation, visualization
M.L.G.: Project administration, validation, supervision.

References

Bishop, C.M. 2006. Pattern Recognition and Machine Learning. Springer.

Breiman, L. 2001. Random forests. *Machine Learning*, vol. 45, no. 1, pp. 5–32. https://doi.org/10.1023/A:1010933404324

Boser, B.E., Guyon, I.M., and Vapnik, V.N. 1992. A training algorithm for optimal margin classifiers. *Proceedings of the Fifth Conference on Computational Learning Theory*. Haussler, D. (ed.). Association of Computing Machinery Press, New York. pp. 144–152.

Cox, D. 1958. The regression analysis of binary sequences. *Journal of the Royal Statistical Society: Series B (Methodological)*, vol. 20, no. 2, pp. 215–232.

Cover, T, and Hart, P. 1967. Nearest neighbor pattern classification. *IEEE Transactions on Information Theory*, vol. 13, no. 1, pp. 21–27. https://doi.org/10.1109/TIT.1967.1053964

Dumont, J.-A., Lemos Gazire, M., and Robben, C. 2017. Sensor-based ore sorting methodology investigation applied to gold ores. *Proceedings of Procemin Geomet 2017*. Gecamin, Santiago, Chile.

Duda, R.O., Hart, P.E., and Stork, D.G. 2001. Pattern Classification. (2nd edn). Wiley-Interscience.

Fisher, R.A. 1936. The use of multiple measurements in taxonomic problems. *Annals of Eugenics,* vol. 7, no. 2, pp. 179-188.

Freund, Y. and Schapire, R.E. 1996. Experiments with a new boosting algorithm. *ICML '96: Proceedings of the Thirteenth International Conference on Machine Learning*, Bari, Italy. Morgan Kaufmann, San Francisco, CA. pp. 148–156.

Gülcan, E. 2020. A novel approach for sensor-based sorting performance determination. *Minerals Engineering*, vol. 146. 106130. https://doi.org/10.1016/j.mineng.2019.106130

Harbeck, H. 2004. Classification of minerals with the use of X-ray transmission. *Proceedings of Kolloquim Sensorgestützte Sortierung*, Clausthal-Zellerfeld.

Jong, T.P.R. and Harbeck, H. 2005. Automated sorting of minerals: Current status and future outlook. *Proceedings. of the 37th Canadian Mineral Processors Conference*. CIM, Montreal. pp. 629–648.

Lechuti-Tlhalerwa, R., Coward, S., and Field, M. 2019. Embracing step-changes in geoscientific information for effective implementation of geometallurgy. *Journal of the Southern African Institute of Mining and Metallurgy*, vol. 119, no. 4. https://doi.org/10.17159/2411-9717/588/2019

Lessard, J., de Bakker, J., and McHugh, L. 2014. Development of ore sorting and its impact on mineral processing economics. *Minerals Engineering*, vol. 65, pp. 88–97. https://doi.org/10.1016/j.mineng.2014.05.019

Li, G., Klein, B., Sun, C., and Kou, J. 2020. Applying receiver-operating-characteristic (ROC) to bulk ore sorting using XRF. *Minerals Engineering*, vol. 146, 106117. https://doi.org/10.1016/j.mineng.2019.106117

Magalhães, M.F., Lemos, M.G., Moreira, V.A., and Pereira, M.S. 2019. O uso de tecnologia ore sorting para aumento em recuperação de Au em minério de transição [The use of ore sorting technology for increased Au recovery in transition ore]. *Proceedings of XXVIII ENTMME*. pp. 1–8. http://www.entmme2019.entmme.org/trabalhos/180.pdf

Manouchehri, H.-R. 2003. Sorting: Possibilities, limitations and future. *Proceedings of Konferens i Mineralteknik*. Föreningen Mineralteknisk Forskning, Stockholm. pp. 1–2.

McCulloch, W.S. and Pitts, W. 1943. A logical calculus of the ideas immanent in nervous activity. *Bulletin of Mathematical Biophysics*, vol. 5, no. 4, pp. 115–133.

Ooms, D., Palm, R., Leemans, V., and Destain, M.-F. 2010. A sorting optimization curve with quality and yield requirements. *Pattern Recognition Letters*, vol. 31, no. 9, pp. 983–990. https://doi.org/10.1016/j.patrec.2009.12.015

Quinlan, R. 1986. Induction of decision trees. *Machine Learning*, vol. 1, no. 1, pp. 81-106.

Reunanen, J. 2012. Overfitting in feature selection: Pitfalls and solutions. Doctoral thesis, Aalto University School of Science, Espoo, Finland. http://lib.tkk.fi/Diss/2012/isbn9789526045160/isbn9789526045160.pdf

Strydom, H. 2010. The application of dual energy X-ray transmissions sorting to the separation of coal from torbanite. Master's thesis, Faculty of Engineering and the Built Environment, University of the Witwatersrand. http://hdl.handle.net/10539/9804

Tusa, L., Kern, M., Khodadadzadeh, M., Blannin, R., Gloaguen, R., and Gutzmer, J. 2020. Evaluating the performance of hyperspectral short-wave infrared sensors for the pre-sorting of complex ores using machine learning methods. *Minerals Engineering*, vol. 146, 106150. https://doi.org/10.1016/j.mineng.2019.106150

Veras, M.M., Young, A.S., Born, C.R., Szewczuk, A., Bastos Neto, A.C., Petter, C.O., and Sampaio, C.H. 2020. Affinity of dual energy X-ray transmission sensors on minerals bearing heavy rare earth elements. Minerals Engineering, vol. 147, 106151. https://doi.org/10.1016/j.mineng.2019.106151

Von Ketelhodt, L. 2009. Viability of optical sorting of gold waste rock dumps. *Proceedings of World Gold Conference 2009*. World Gold Council, London. pp. 271–278.

Von Ketelhodt, L. and Bergmann, C. 2010. Dual energy X-ray transmission sorting of coal. *Journal of the Southern African Institute of Mining and Metallurgy*, vol. 110, no. 7, pp. 371–378.

Webb, A.R. and Copsey, K.D. 2011. Statistical Pattern Recognition. Wiley. https://doi.org/10.1002/9781119952954

Wills, B.A. and Finch, J. 2015. Wills' Mineral Processing Technology: An Introduction to the Practical Aspects of Ore Treatment and Mineral Recovery. Butterworth-Heinemann. ◆